JOURNAL OF APPLIED ELECTROCHEMISTRY 20 (1990) 281–288

In situ activation of nickel cathodes by sodium molybdate during alkaline water electrolysis at constant current

J. -Y. HUOT*, L. BROSSARD

Institut de recherche d'Hydro-Québec, 1800 montée Ste-Julie, Varennes, Québec, Canada J0L 2P0

Received 6 January 1989; revised 25 May 1989

The nickel cathode undergoes significant deactivation at 100 mA cm^{-2} in 30 wt % KOH at 70° C containing KOH metallic impurities. The time dependence of the potential reveals two distinct regions: the first due to hydrogen absorption, while the Tafel parameters, charge transfer resistance and double-layer capacitance remain fairly constant; the second due to the electrodeposition of metallic impurities as manifested by SEM pictures, EDX analysis and cyclic voltammograms. The resulting deactivation is due mainly to the increase in the Tafel slope, although the electrode impedance reveals a significant increase in electrode roughness. The hydrogen discharge at 100 mA cm^{-2} in 30 wt % KOH containing 4 mM sodium molybdate largely attenuates the deactivation process owing to hydrogen absorption and the deposition of impurities. The *in situ* activation is ascribed to the formation of a spongy molybdenum-base deposit on the nickel cathode during the first day of water electrolysis.

1. Introduction

In a strongly alkaline solution at 70° C, the nickel electrode undergoes significant deactivation during hydrogen discharge in constant current or constant potential mode [1]. Reactivation is observed when a certain amount of sodium molybdate is dissolved in the electrolytic solution and the applied cathodic overpotential is high with respect to the hydrogen evolution reaction (HER) [1, 2]. This *in situ* activation is attributed to the electrodeposition of metallic molybdenum on the nickel surface during hydrogen evolution at high current densities, e.g. 100 mA cm^{-2}.

Several authors have studied the physicochemical properties of molybdate and its ability to modify the surfaces of electrodes. It has been demonstrated that among various molybdate species such as monomer MoO_4^{2-}, monoprotonated and diprotonated monomers and isopolymolybdates, monomer MoO_4^{2-} alone is present in alkaline solutions whereas a mixture of these species prevails in acid solution [3]. Cathodic polarization of acid molybdate solutions produces molybdenum-modified electrodes, thereby promoting the catalytic activity of electrochemical oxidation of methanol [4]. Methanol oxidation is thought to be catalysed by the strongly adsorbed redox couple Mo(IV)/Mo(III). Meanwhile, passivation coatings of Mo(V) and Mo(IV) species have been developed by cathodic reduction of sodium molybdate solutions between pH 1 and 13 [5]. For the HER in particular, activation of graphite cathodes by electroreduction of molybdate in alkaline solutions has already been reported [6]. Compared to graphite, molybdenized graphite shows a 200 mV improvement in its overpotential at 250 mA cm^{-2}. This is ascribed to (i) the reduction of molybdate in an adherent brown molybdenum oxide [6–8] and (ii) further reduction of this oxide by atomic hydrogen, since cathodic preparation of metallic molybdenum was indirect.

An electrocatalytic effect is induced when sodium molybdate and *tris*-ethylenediamine cobalt (III) chloride are mixed at about 10^{-2} M [7, 8]. This effect is attributed to a Mo–Co synergic codeposit which appears to be active as long as the cathodic current flows; dissolution is observed immediately after interruption of the electrolysis. *In situ* activation depends on the electrode matrial and the resulting Co–Mo–Ni and Co–Mo–Fe cathodes are shown to be the most active. The authors point out that codeposition of Mo and Co promotes the reduction of molybdate. *In situ* activation reaches maximum activity after two days at 300 mA cm^{-2}, after which the applied potential remains constant for two months [7].

Furthermore, *in situ* electrodeposition of nickel on vitreous carbon has already been achieved for the electrocatalytic hydrogenation of organic molecules in acidic media [9]. The hemispherical nickel centres obtained showed Tafel parameters for the HER comparable to those of smooth nickel. A significant improvement is observed for the HER when the *in situ* activation of various electrode materials is carried out with iso- and heteropolyanions of tungsten (VI) or monotungstate WO_4^{2-} [10, 11]: the exchange current density reaches 3 to 5 mA cm^{-2} on the modified electrode. Hydrogen evolution and the reduction of the tungsten salt are both obtained at constant applied cathodic potential.

The present investigation is devoted to the deacti-

* Present address: Noranda Technology Centre, 240 Hymus boul., Pointe Claire (Qué) Canada H9R 1G5.

0021-891X/90 $03.00 + .12 © 1990 Chapman and Hall Ltd.

vation process of a nickel cathode and its *in situ* activation by sodium molybdate at low hydrogen overpotentials and a current density of 100 mA cm^{-2}. Measurements of the time dependence of the potential, Tafel lines and impedance, cyclic voltammetry and surface analysis were performed in 30 wt % KOH at 70° C, that is the operating conditions of the experimental electrolysis plant located on the IREQ site in Varennes [12].

2. Experimental

The electrochemical measurements were performed at 70° C in 30 wt % KOH containing KOH impurities such as iron (0.5 ppm) and nickel (0.6 ppm) [1]; the electrolyte solution was not purified so that one could obtain, as closely as possible, the composition of the electrolyte prevailing in the experimental electrolysis plant. The electrochemical methods, the chemicals and the cell are described in detail elsewhere [1, 2]. The working electrode was controlled by a 1286 Solartron Electrochemical Interface and the impedance was measured at 100 mA cm^{-2} with a 1250 Solartron Frequency Analyser. Each impedance plot ranged from 10 Hz to 65 kHz using 16 frequencies per decade.

The working electrode consisted of a vertical nickel wire (Mt. Res. Corp. 99.99%) 0.05 cm in diameter, polished with alumina paste (1 μm) prior to the electrochemical experiments. All potentials are given with respect to the Hg/HgO/1 M KOH reference electrode at 23° C. The measured value of the reversible potential for the hydrogen reaction in 30 wt % KOH, 70° C was -0.960 V with respect to this electrode. *E–i* curves were obtained by a standard galvanodynamic technique at a sweep rate of 0.2 mA cm^{-2} s^{-1} in the direction of decreasing current values from 100 to 1 mA cm^{-2} after the working electrode had been held at 100 mA cm^{-2} for a given time.

3. Results and discussion

3.1. *Constant applied potential mode*

In situ activation of a nickel cathode depends on the concentration of sodium molybdate [2] and on the applied cathodic potential (Fig. 1a). This process is well illustrated by the time dependence of the current density difference (ΔI) between polarizations with and without molybdate (Fig. 1b) at the same potential.

Before *in situ* activation occurs, all electrodes under polarization undergo a deactivation in 30 wt % KOH in the presence of 4 mM sodium molybdate at 70° C. The reactivation rate and magnitude are dependent on the applied potential. The steady state is reached in times ranging from 10^4 to 4×10^4 s. The small increase in ΔI at -1.4 V after 10^4 s is related to a slight *in situ* activation resulting from a deposition of iron in the absence of sodium molybdate.

The nickel cathode becomes strongly deactivated after several days at $-1.5\,V_{Hg/HgO}$ in 30 wt % KOH free of dissolved molybdate. After 3 days, the hydrogen overpotential at 250 mA cm^{-2} (η_{250}) calculated from the Tafel slope b = 145 mV and the exchange current density i_0 = 0.09 mA cm^{-2} is 500 mV while the electrode surface is covered by an iron-rich deposit. After 3 days of electrolysis under the same experimental conditions (except that 4 mM of molybdate is present in the alkaline solution), b = 123 mV and i_0 = 3.28 mA cm^{-2} and η_{250} is reduced to 231 mV. The resulting electrode surface is covered entirely with a spongy film of molybdenum, iron and copper.

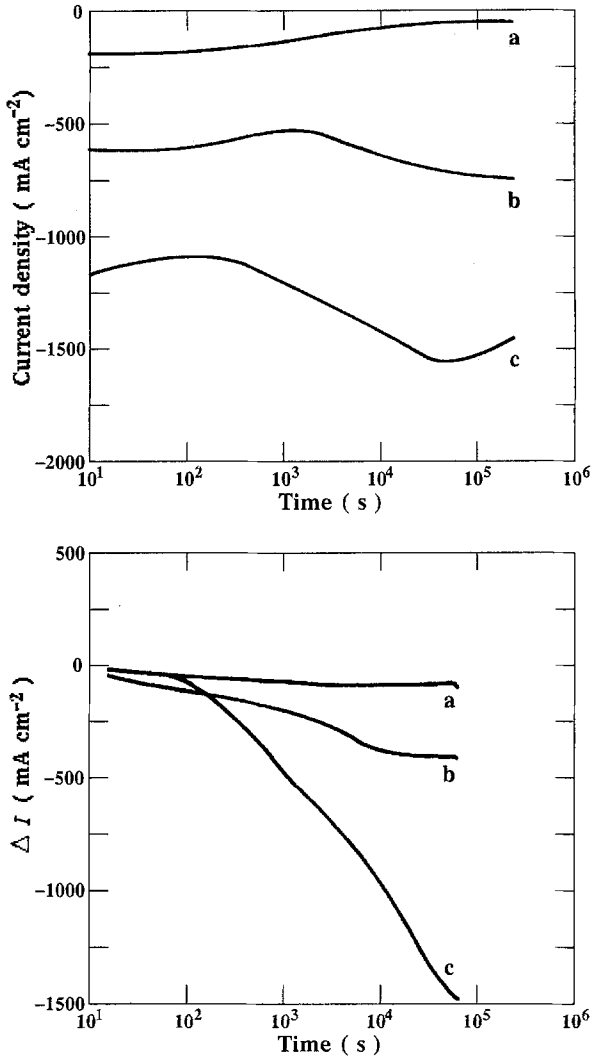

Fig. 1. Time dependence of the current density with 4 mM dissolved sodium molybdate and current density difference (ΔI) with and without dissolved sodium molybdate at (a) -1.3, (b) -1.4 and (c) -1.5 V for nickel cathode in 30 wt % KOH at 70° C.

By comparison, after 3 days at $-1.3\,V_{Hg/HgO}$ in 30 wt % KOH containing 4 mM of molybdate, b = 173 mV, i_0 = 1.57 mA cm^{-2} and η_{250} is 379 mV. The electrode is partially covered with a dispersed deposit composed of iron, copper and zinc, accounting for the high exchange current density. The absence of deposited molybdenum at -1.3 V is supported by cyclic voltammetry performed at a sweep rate of 10 mV s^{-1} after 3 days at $-1.3\,V_{Hg/HgO}$, whereas after 3 days at $-1.5\,V_{Hg/HgO}$ the cyclic voltammogram reveals that 4 C cm^{-2} of molybdenum is deposited. In summary, *in situ* activation by molybdate occurs only for potentials cathodic or equal to -1.3 V, and its rate

and magnitude are strongly dependent on the potential. An applied potential dependence of *in situ* activation was also observed for the cobalt cathode under the same experimental conditions [13].

3.2. *Deactivation and* in situ *activation at constant current density*

A deactivation is reported at constant current and could be assimilated to a potential shift toward more cathodic potentials [1]. From the time and potential dependences of the activity shown in Fig. 1, it can be anticipated that the galvanostatic *in situ* activation process at 100 mA cm^{-2} will begin between -1.3 and $-1.4\,V_{Hg/HgO}$ and after 10^3 to 10^5 s of electrolysis. As a matter of fact, this behaviour was observed for nickel cathodes at 37° C in 30 wt % KOH containing 3 ppm iron [14].

The time dependence of the potential of the smooth nickel cathode at 250 mA cm^{-2} at 70° C in 30 wt % KOH containing only KOH metallic impurities such as iron (0.5 ppm) clearly reveals that a deactivation process occurs, as manifest by two distinct regions labelled I and II in Fig. 2, curve a. In addition, the absence of deposited impurities on the electrode in region I was shown by cyclic voltammetry performed at a sweep rate of 10 mV s^{-1} (Table I). Only region I was observed in a previous work on nickel at 37° C [15], possibly because the galvanostatic experiment was performed for only 5×10^4 s.

Permeation measurements have revealed that hydrogen absorption and β-hydride formation are responsible for this first increase in cathode potential [16]. In agreement with this statement, and by analogy with potentiostatic deactivation, which also occurs in two distinct regions [1], the process of galvanostatic deactivation in region I is ascribed to hydrogen penetration in the metal lattice.

Table 1. Parameters variation during galvanostatic deactivation at 100 mA cm^{-2}

Time (s)	i_0^* *(10^5 A cm^{-2})*	*b (mV)*	$\eta_{obs}^{\dagger}$ *(mV)*	η_{calc} *(mV)*	$Q_{Fe}^{\ddagger}$ *(mC cm^{-2})*
10^2	4.6	102	304	340	0
10^3	2.7	99.7	344	356	0
10^4	4.8	116	404	385	0
5.0×10^4	14	133	434	380	1
7.5×10^4	25	166	454	432	2.5
10^5	10	140	484	420	26§
2.4×10^5	7.5	182	529	569	30§

* Obtained by current density sweep from 100 to 1 mA cm^{-2} at a rate of 0.2 mA cm^{-2} s^{-1}.
† Experimental value of the potential minus the reversible hydrogen electrode potential and ohmic drop (6 mV).
‡ Charge of the anodic peak at -0.5 V determined by cyclic voltammetry at 10 mV s^{-1} between -1.3 and $+0.7\,V_{Hg/HgO}$ and attributed to iron oxidation.
§ An additional anodic peak is observed at -0.26 V ($Q \approx 10$ mC cm^{-2}).

Region II is associated with the electrodeposition of an iron-rich deposit on the nickel electrode (Table I, Fig. 3) in agreement with the second potentiostatic deactivation region for which such an iron deposit was also observed [1]. Experiments carried out for 10^5 s at 250 mA cm^{-2} and 37° C exhibit a monotonic deactivation of the nickel cathode in the presence of 0.03 ppm dissolved iron [14]. With 3.0 ppm dissolved iron, deactivation is followed by reactivation beginning during iron electrodeposition at ~ 5000 s of polarization and having approximately the same magnitude as the deactivation process. For 0.5 ppm dissolved iron, the potential–time curve (curve a, Fig. 1) is intermediate to those mentioned above. The transition between regions I and II at $\sim 10^4$ s may therefore be correlated with the start of iron electrodeposition, whereas additional metallic deposition seems to be responsible for further deactivation.

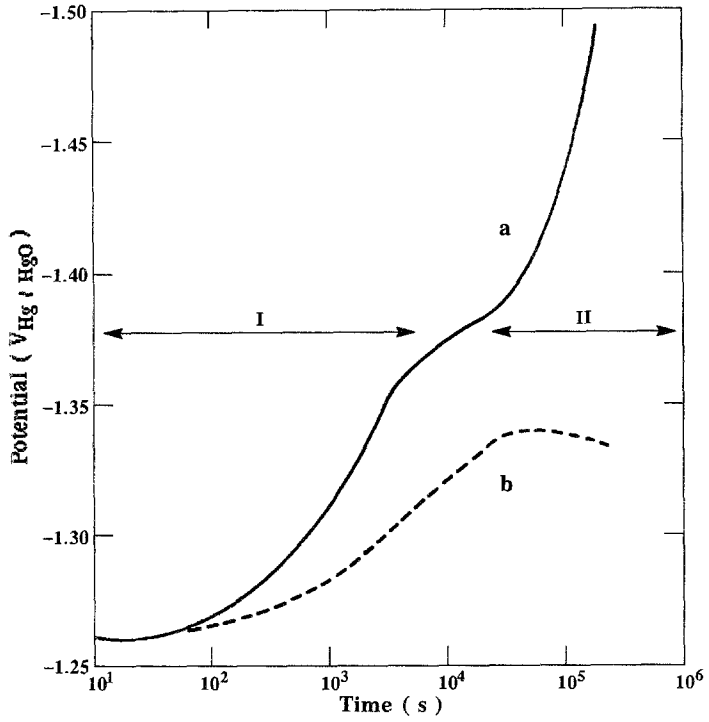

Fig. 2. Time dependence of the cathode potential at 100 mA cm^{-2} with (– – –) and without (———) 4 mM sodium molybdate for a nickel cathode in 30 wt % KOH.

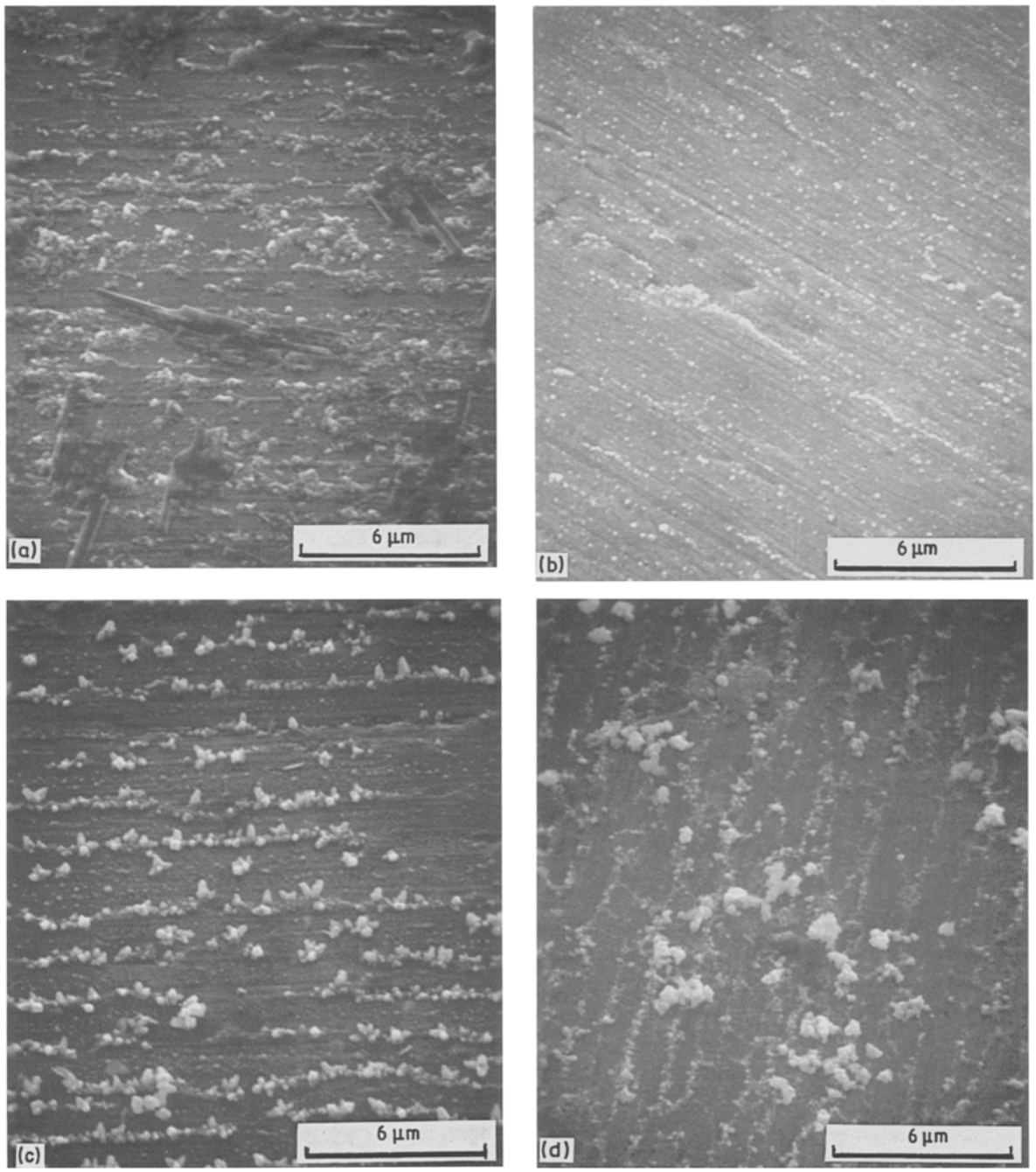

Fig. 3. SEM pictures after various times at 100 mA cm^{-2} for a nickel cathode in 30 wt % KOH free solution molybdate, 70° C: (a) 7.5 × 10^4, (b) 10^5, (c) 1.6 × 10^5, and (d) 2.4 × 10^5 s. EDX analysis (at %) of the surface: (a) Ni 97.9, Fe 2.1; (b) Ni 92.5, Fe 3.4, Cu 4.1; (c) Ni 90.3, Fe 4.1, Cu 2.3, Zn 3.3; (d) Ni 89.0, Fe 5.9, Cu 3.5, Zn 1.6.

In the absence of sodium molybdate, the amount of metallic impurities deposited on the Ni cathode (Fig. 3) increases with time in region II while the electrode potential for the HER shifts with time in the cathode direction (Fig. 2). The transition between galvanostatic deactivation regions I and II was associated with the beginning of metal deposition on the surface and is characterized by an increase in the Tafel slope. Region II may be associated with the growth of a dispersed weakly active metallic deposit.

The time dependence of the cathode potential at 100 mA cm^{-2} in the presence of 4 mM $Na_2Mo_4 2H_2O$ (Fig. 2, curve b) reveals that an *in situ* activation process starts at 100 s. The E against log t relationship shows that the deactivation process in region I is largely attenuated and that it is followed by a large reaction process which completely hides region II.

The time dependence of the electrode potential is also influenced by metallic components other than molybdenum which are simultaneously deposited on the nickel cathode during electrolysis (Fig. 4). Cyclic voltammetry (Table 2) and X-ray microanalysis (Fig. 4) indicate that *in situ* electrodeposition starts after 10^4 s, the potential being close to $-1.33\ V_{Hg/HgO}$, which corresponds to the onset of *in situ* activation (Fig. 2). These time and potential thresholds are in agreement with those anticipated from analysis of the potential dependence of the reactivation process presented in the previous section. Because the active molybdenum coating was found to be unstable, it is

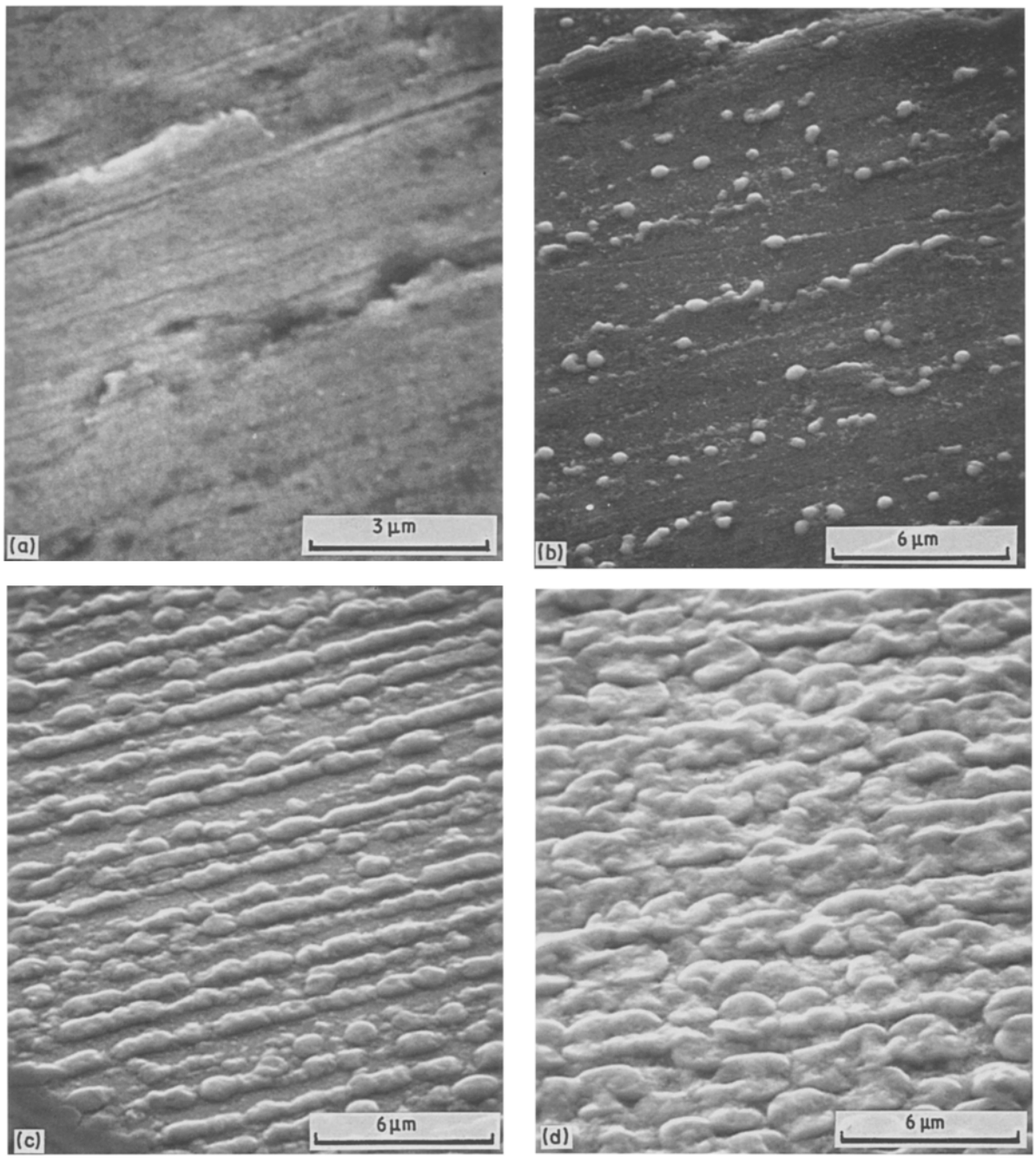

Fig. 4. SEM pictures after various times at 100 mA cm^{-2} for a nickel cathode in 30 wt % KOH containing 4 mM sodium molybdate, 70° C: (a) 7.5 × 10^4, (b) 5 × 10^4, (c) 10^5 and (d) 2.4 × 10^5 s. EDX analysis (at %) of the surface: (a) Ni 99.5, Mo 0.5; (b) Ni 95.1, Mo 2.6, Fe 1.1, Cu 1.2; (c) Ni 76.6, Mo 12.2, Fe 9.3, Cu 1.9; (d) Ni 53.8, Mo 23.9, Fe 19.9, Cu 2.4.

interesting to note that the current deposit is sufficiently stable to be studied *in situ* by cyclic voltammetry or *ex situ* by SEM and EDX, following interruption of the electrolysis. This stabilization of the Mo-base deposit may be attributed to alloying with Fe, Cu, Zn and perhaps the Ni substrate.

In the presence of sodium molybdate, the electrode potential and the Tafel parameters are substantially different from those obtained in the absence of dissolved sodium molybdate. For instance, metallic elements are detectable on the surface for $t = 10^4$ s (Fig. 4, Table 2) while i_0 and b are significantly larger, at any time, in the presence of dissolved molybdate. Significant modifications in the surface morphologies and composition (Fig. 4) are observed between 10^4 and 2.4 × 10^5 s, whereas the electrode potential and corresponding Tafel parameters (Table 2) remain unchanged.

The time dependence of the electrocatalytic activity (Figs 1, 2) suggests that the final state of the surface corresponds to an active metallic form of Mo with mixed metals arising from the indirect reduction of deposited intermediate oxides by the adsorbed atomic hydrogen during the intense hydrogen discharge [7].

The overpotential dependence of the slope $\partial I/\partial \log t$ (Fig. 1b) or the activation observed when the potential reaches values higher than − 1.3 V (Fig. 2) is tentatively explained by the increased hydrogen activity on the surface (i.e. hydrogen coverage) as the hydrogen overpotential becomes more cathodic. Consequently, the

Table 2. Parameter variation during in situ *activation at 100 mA cm^{-2} in the presence of 4 mM sodium molybdate*

Time (s)	i_0^* *(10^5 A cm^{-2})*	*b (mV)*	$\eta_{obs}^{\dagger}$ *(mV)*	η_{calc} *(mV)*	$Q_{Mo}^{\ddagger}$ *(mC cm^{-2})*	Q_{Fe}
10^2	65	160	310	350	0	0
10^3	90	178	340	364	0	0
10^4	65	178	370	389	< 1	< 1
5.0×10^4	50	168	370	386	6	2
10^5	45	152	369	357	215	10
2.4×10^5	33	141	360	350	1000	25

* Obtained by current density sweep from 100 to 1 mA cm^{-2} at a rate of 0.2 mA cm^{-2} s^{-1}.
† Experimental value of the potential minus the reversible hydrogen electrode potential and ohmic drop (6 mV).
‡ Charge of the anodic peaks determined by cyclic voltammetry at 10 mV s^{-1} between −1.3 and +0.7 $V_{Hg/HgO}$ and attributed to iron and molybdenum oxidation; $E_{p(Mo)} = -830$ mV; $E_{p(Fe)} = -470$ mV.

kinetics of the indirect reduction of molybdenum oxide(s) could be accelerated at more negative values of the applied overpotential. The oxidation state of the molybdenum in the deposit is clearly indicated in cyclic voltammetry, because its potential peak is the same as the potential of the metallic Mo oxidation.

It is therefore deduced that hydrogen evolution takes place on a metallic Mo alloy having a composition which changes during water electrolysis. Unfortunately, the surface stability of the Mo-base deposit resulting from the alloying with iron and copper makes the deposit less active than other unstable Mo deposits [6–8] for the HER.

3.3. *Impedance measurements*

Impedance measurements were performed from 10 Hz to 65 kHz at different times during the water electrolysis at 100 mA cm^{-2} in the absence and presence of sodium molybdate. In a different set of experiments, it was established from the E against log t curve and the impedance diagram that the effects of a 1000 Hz superimposed signal on the HER kinetics are negligible; the frequency sweep performed after 4×10^4 s results in the same diagram, whether this sweep is the first or the ninth.

Under these experimental conditions, a simple RC behaviour is observed (Fig. 5). From the experimental

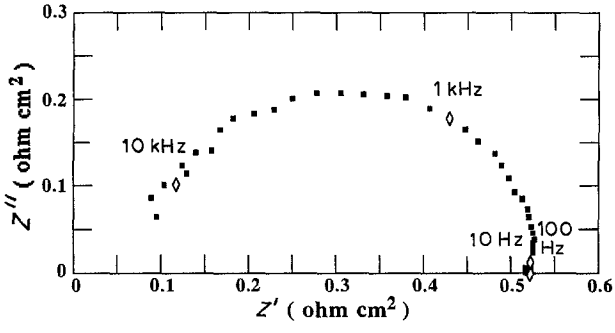

Fig. 5. Impedance plot for a nickel cathode after 100 s of hydrogen discharge at 100 mA cm^{-2} in 30 wt % KOH containing 4 mM sodium molybdate.

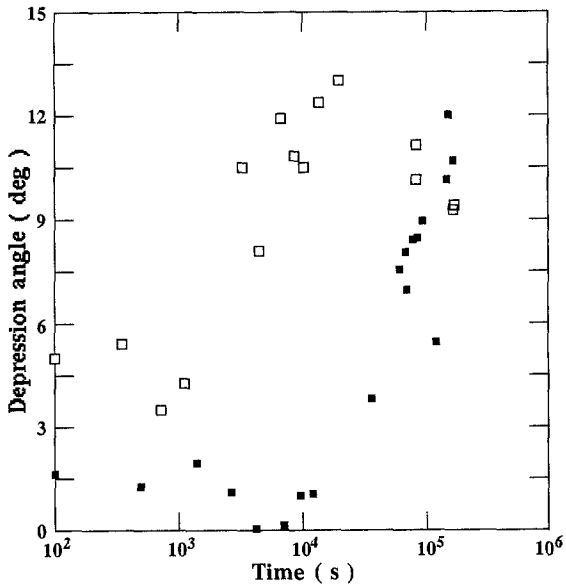

Fig. 6. Time dependence of the depression angle at 100 mA cm^{-2} with (□) and without (■) 4 mM sodium molybdate for nickel cathode in 30 wt % KOH at 70° C.

impedance diagram Z′–Z″, the charge transfer resistance R_{ct}, the double-layer capacitance C_{dl}, the ohmic resistance R_s, and the depression angle θ are evaluated given as a function of the electrolysis time (Figs 6–8).

The depression angle remains negligible up to 10^4 s at 100 mA cm^{-2} and increases to approximately 10° after 10^5 s in the absence of sodium molybdate (Fig. 6). A slightly different trend is observed in the presence of molybdate since this angle increases after only 3000 s. It was pointed out [17] that the displacement of the centre of the experimental arc below the real axis may be ascribed to an increase in surface roughness. For a surface containing pores and defects of various shapes, diameters and depths, the charging wave reaches different penetration depths at different frequencies resulting in a distribution of the time con-

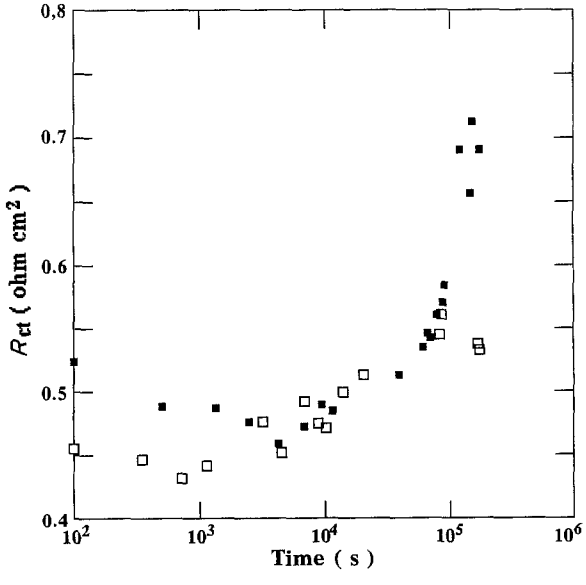

Fig. 7. Time dependence of the charge transfer resistance at 100 mA cm^{-2} with (□) and without (■) 4 mM sodium molybdate for nickel cathode in 30 wt % KOH at 70° C.

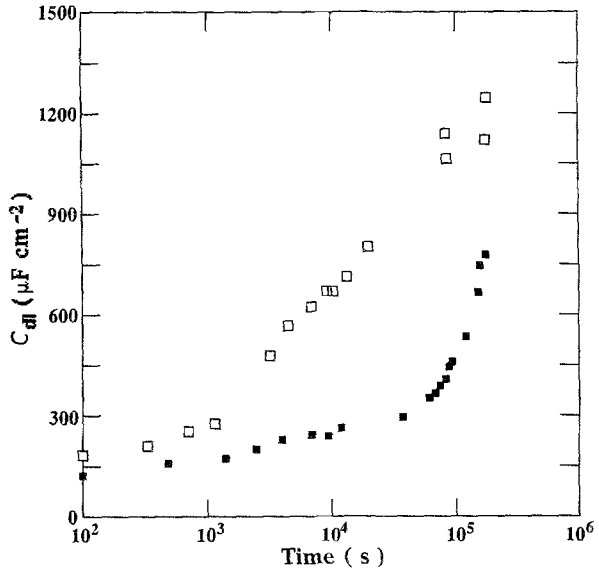

Fig. 8. Time dependence of the double-layer capacitance at 100 mA cm^{-2} with (□) and without (■) 4 mM sodium molybdate for nickel cathode in 30 wt % KOH at 70° C.

stant [18]. Thus, the angle θ is related to the width of the relaxation time distribution [19]. In the present case, the increase in the depression angle is indicative of a significant increase in surface roughness during hydrogen discharge, as evidenced by the detection of a deposit on the electrode (Figs 3 and 4).

In the case of rough surfaces, direct comparison of the apparent C_{dl} of the electrode with that of a flat electrode will not give a meaningful estimate of the electrochemically active surface area, because the apparent C_{dl} varies with the frequency. However the C_{dl} variation for a given electrode material under similar conditions may be used for an estimate of the roughness [17] even if the surface composition is modified during electrolysis because the electrode capacitance is weakly affected by the change in surface composition [20].

The variation of the charge transfer resistance (Fig. 7) and double layer capacitance (Fig. 8) with time in the absence of molybdate follows the same trend as that for the consumed-charge against log t curve. The trend for R_{ct} means that the HER is practically unaffected for times shorter than 5×10^4 s and that a significant deactivation occurs after this time, as shown by the variation in the potential against time (Fig. 2, curve a). This is in agreement with the slight time dependence of the Tafel parameters in region I ($t \leqslant 5.0 \times 10^4$ s) (Table 1). For the polished nickel cathodes, the R_{ct} value at 100 mA cm^{-2} is similar to that previously reported at high cathodic overpotentials [21]. Except during long periods of electrolysis, the charge transfer resistance is not affected by the presence of molybdate in 30 wt % KOH, as supported by the calculated overpotentials (Tables 1 and 2). For times exceeding 10^5 s at 100 mA cm^{-2}, R_{ct} remains relatively constant in the presence of molybdate whereas the observed and calculated overpotentials decrease slightly; this is attributed to an *in situ* activation.

The C_{dl}-time curve (Fig. 8) indicates that region I of the deactivation process in the absence of molybdate is not related to a decrease in initial surface area. Moreover, the formation of a larger surface area is supported when metallic impurities are deposited on the nickel cathode during the early stages of the deactivation process in region II (Fig. 4). This means that the second deactivation process is due essentially to the deposition of an alloy that is less active than the smooth nickel. The magnitude of C_{dl} for the freshly polished nickel cathode at 100 mA cm^{-2} is similar to that observed between 300 and 400 mV cathodic overpotential under similar experimental conditions [21].

For platinum cathodes in 1 M HCl, pronounced time effects were reported for C_{dl} and R_{ct} during the first hour of potentiostatic deactivation [22]. The increase in R_{ct} and decrease in C_{dl} were associated with the bubble formation and detachment mechanism. In the present cases, no such effect can be observed because of the relative constancy of the ohmic resistance, $R_s = 0.06 \pm 0.01\,\Omega\,\text{cm}^2$, during both steps of the deactivation process. In addition, the time constant of the relaxation process associated with the bubble layer on nickel cathodes [23] is such that this phenomem is largely completed before the first impedance measurement at 100 s.

The presence of sodium molybdate results in a large C_{dl} value (Fig. 8) during hydrogen discharge at 100 mA cm^{-2}, suggesting the rapid formation of a rough molybdenum-base deposit which modifies the HER mechanism without substantially changing the kinetic rate of the charge transfer.

This is supported by the large Tafel slope and exchange current density for HER (Table 2) — in spite of the physical complexity of the i_0 parameter — by the depression angle θ and, subsequently, by the SEM pictures and EDX analyss. The C_{dl} difference with and without molybdate (Fig. 8) starts to increase after 10^4 s, indicating a significant change in the surface electrode composition and mostly its morphology. The latter effect is well supported by the SEM pictures (Figs 3 and 4).

4. Conclusion

The nickel cathode undergoes a significant deactivation process at 100 mA cm^{-2} in 30 wt % KOH at 70° C containing KOH metallic impurities, as manifested by the time dependence of the potential in two distinct regions. Region I shows a total increase of 120 mV in the cathode overpotential, which is attributed to hydrogen penetration in the nickel lattice, whereas the Tafel parameters, charge transfer resistance and double-layer capacitance vary only slightly. Region II is attributed to the electrodeposition of metallic impurities, as revealed by SEM pictures, EDX analysis and cyclic voltammograms. The resulting deactivation by the metallic deposit is mainly due to the increase in the Tafel slope. Although the electrode impedance reveals a significant increase in elec-

trode roughness, the exchange current density remains fairly constant.

The hydrogen discharge at 100 mA cm^{-2} in 30 wt % KOH containing 4 mM sodium molybdate largely attenuates the deactivation process owing to the hydrogen absorption, eliminates region II associated with the deposition of impurities and results in a very slight time dependence of the potential. This *in situ* activation is ascribed to the formation of a spongy molbdenum-base deposit on the nickel cathode during the first day of water electrolysis. The Tafel parameters and the charge transfer resistance are in agreement with the small variation in cathode overpotential, whereas the electrocatalytic activity of this deposit is related mostly to its roughness, as suggested by the time variation of the double-layer capacitance.

References

[1] J.-Y. Huot and L. Brossard, *Int. J. Hydrogen Energy* **12** (1987) 821.
[2] *Idem, Surf. Coat. Technol.* **34** (1988) 373.
[3] T. Ozeki, H. Kihara and S. Ikeda, *Anal. Chem.* **60** (1988) 2055.
[4] K. Kita, H. Nakajima and K. Shimazu, *J. Electroanal. Chem.* **248** (1988) 181.
[5] G. D. Wilcox, D. R. Gabe and M. E. Warwich, *Corrosion Sci.* **28** (1988) 577.
[6] M. M. Jaksic and I. M. Csonka, *Electrochem. Technol.* **4** (1966) 49.
[7] C. M. Lacnjevac and M. M. Jaksic, *R. Res. Inst. Catal. Hokkaido Univ.* **31** (1983) 7.
[8] C. M. Lacnjevac, N. M. Markovic and M. M. Jaksic, *Surf. Technol.* **22** (1984) 51.
[9] M. J. Lain and D. Pletcher, *Electrochim. Acta.* **32** (1987) 99, 109.
[10] B. Keita and L. Nadjo, *Electroanal. Chem.* **191** (1985) 441.
[11] *Idem, ibid.* **227** (1987) 265.
[12] R. L. LeRoy and A. F. Hufnagl, *Int. J. Hydrogen Energy* **8** (1983) 581.
[13] J.-Y. Huot and L. Brossard, *J. Appl. Electrochem.* **18** (1988) 815.
[14] M. A. Riley and P. J. Moran, *J. Electrochem. Soc.* **133** (1986) 760.
[15] H. E. G. Rommel and P. J. Moran, *ibid.* **132** (1985) 325.
[16] *Idem, ibid* **135** (1988) 343.
[17] U. Rammelt and G. Reinhard. *Corros. Sci.* **27** (1987) 373.
[18] R. De Levie, in 'Advances in Electrochemistry and Electrochemical Engineering', Vol. 6, Wiley, New York (1967) p. 329.
[19] J. R. MacDonald (Ed.) 'Impedance spectroscopy' Wiley, New York (1987).
[20] M. A. Vorotyntev, in 'Modern Aspects of Electrochemistry', J. O'M. Bockris, B. E. Conway and R. E. White (Eds.), Vol. 17, Plenum Press, New York (1986), Chap. 2.
[21] J.-Y. Huot, *J. Electrochem. Soc.* **136** (1989) 1933.
[22] J. A. Harrison and A. T. Kuhn, *Surf. Technol.* **19** (1983) 249.
[23] J.-Y. Huot, *J. Appl. Electrochem.* **19** (1989) 453.